Elastic oscillations of cylindrical fuses

G. D. Mahan[a)]
Department of Physics, University of Tennessee, Knoxville, Tennessee 37996-1501 and Solid State Division, Oak Ridge National Laboratory, Oak Ridge, Tennessee 37831-6032

J. R. Gladden and J. D. Maynard
Department of Physics and Astronomy, Pennsylvania State University, 104 Davey Laboratory, University Park, Pennsylvania 16802

(Received 17 June 2001; accepted for publication 16 July 2001)

A fast current pulse causes a material to heat and undergo rapid expansion. We calculate the response of a cylindrically shaped material to a pulse on the microsecond time scale. The first step is to obtain the breathing modes of elastic oscillation of the cylinder. These modes are calculated using a Rayleigh–Ritz variational method introduced by Demarest for cubes. The boundary conditions are derived, which give the amplitude of each elastic mode in response to the sudden heating. The results are illustrated by calculations on a station arrester made of a ZnO ceramic. © *2001 American Institute of Physics.* [DOI: 10.1063/1.1402148]

I. INTRODUCTION

Zinc oxide varistors are a type of fuse used to clamp surges in line voltages. A voltage surge in the input line is absorbed in the varistor, causing it to heat rapidly for large surges. A very large surge causes it to break or fail by puncture or fracture.[1] All varistors are cylindrical in shape. Depending upon their use, some are long cylinders while others are short. Recently we have modeled the failures of varistors from the diffusion of heat originating from a current filament.[1,2] The filament is caused by inhomogeneities in the material. Another model for failure was considered by Vojta and Clarke,[3] who assumed the heating was uniform, and the response was due to the excitation of an elastic wave. They were only able to solve the two limiting cases of very long and thin varistors, or very short ones. Here we solve the general case of cylinders with any aspect ratio between length and radius. An entirely numerical solution for a general cylinder was given by Lengauer *et al.*[4]

The present method can be used for any cylindrical object that is heated rapidly. The basic idea is that the cylinder has normal modes of elastic oscillation. The heating pulse causes the cylinder to expand, which excites the breathing modes. Fracture is caused by stresses which exceed a material limit. The largest stresses are found at the largest value of the oscillation amplitudes. Many modes contribute to these oscillations.

Section II solves for the elastic oscillations of a solid cylinder. The oscillations of a finite cylinder have been discussed in a number of books on elasticity.[5–8] They all state that the problem has never been solved. Recently, a numerical solution was presented by Visscher *et al.*[9] Their solution did not allow the discussion of the symmetry of most of the modes and only included one set of Lamé parameters. Here we solve the problem again so that the mode symmetry is obvious.

Some torsional modes have simple analytical solutions, but most breathing modes are quite complicated. The best numerical method is a variation on the Rayleigh–Ritz technique, which has become accessible with the age of the computer. It has been applied to the vibrations of the cube with much success.[10–14]

II. VARIATIONAL METHOD

Here we summarize the variational method. The total energy density of a vibrating harmonic system is the kinetic energy (K) and potential energy (V)

$$K=\frac{\rho_m}{2}\int d^3r\,\dot{\mathbf{u}}\cdot\dot{\mathbf{u}}, \tag{1}$$

$$V=\frac{1}{2}\int d^3r\,\mathbf{u}\cdot\boldsymbol{\mathcal{L}}\cdot\mathbf{u}, \tag{2}$$

$$\mathcal{E}=K+V, \tag{3}$$

where ρ_m is the mass density. The tensor operator $\mathcal{L}$ is specified below. When oscillating the displacement $\mathbf{u}(\mathbf{r},t)=\mathbf{u}(\mathbf{r})\cos(\omega t)$ so the various energies are

$$K=\omega^2 K_s\sin^2(\omega t),\quad K_s=\frac{\rho}{2}\int d^3r\,\mathbf{u}(\mathbf{r})\cdot\mathbf{u}(\mathbf{r}), \tag{4}$$

$$V=V_s\cos^2(\omega t),\quad V_s=\frac{1}{2}\int d^3r\,\mathbf{u}(\mathbf{r})\cdot\mathcal{L}\cdot u(\mathbf{r}), \tag{5}$$

$$\mathcal{E}=\frac{1}{2}\{[\omega^2K_s+V_s]-[\omega^2K_s-V_s]\cos(2\omega t)\}. \tag{6}$$

An accurate solution is obtained by reducing the second bracket to be as small as possible. This idea is the basis of the variational procedure. The function to be minimized is $\mathcal{F}=\omega^2K_s-V_s$. In the Rayleigh–Ritz method, the procedure is to expand the function $\mathbf{u}(\mathbf{r})$ in a set of basis functions

[a)]Author to whom correspondence should be addressed.

$\mathbf{u}_i(\mathbf{r})$ and then perform a variational operation on the coefficients. We select the basis so that they are orthogonal over the volume of the cylinder

$$\mathbf{u}(\mathbf{r})=\sum_{i=1}^{N} A_i\mathbf{u}_i(\mathbf{r}), \quad \int d^3r\, \mathbf{u}_i(\mathbf{r})\cdot\mathbf{u}_j(\mathbf{r})=\delta_{ij}, \tag{7}$$

$$K_s=\frac{\rho_m}{2}\sum_{ij} A_iA_j\int d^3r\, \mathbf{u}_i(\mathbf{r})\cdot\mathbf{u}_j(\mathbf{r})=\frac{\rho_m}{2}\sum_i A_i^2, \tag{8}$$

$$V_s=\frac{1}{2}\sum_{ij} A_iA_jL_{ij}, \quad L_{ij}=\int d^3r\, \mathbf{u}_i(\mathbf{r})\cdot\mathcal{L}\cdot\mathbf{u}_j(\mathbf{r}), \tag{9}$$

$$\frac{\delta\mathcal{F}}{\delta A_i}=0=\rho_m\omega^2A_i-\frac{\delta V_s}{\delta A_i}. \tag{10}$$

The latter equation is a standard eigenvalue equation. The oscillation frequencies ω_i are the square root of the eigenvalues of the matric L_{ij}/ρ_m.

The elastic displacement is a vector $\mathbf{u}(\mathbf{r})$ and the differential equation is a vector wave equation. The boundary conditions are that the stress tensor σ_{ij} obeys $0=\Sigma_i n_i\sigma_{ij}$ where n_i is the vector normal to the surface. There are three components to this equation for each surface. The reason that the problem is difficult to solve is that simple combinations of basis functions do not obey the boundary conditions on all of the surfaces. The interesting aspect of the variational method is that the perfect variational solution automatically obeys the stress-free boundary conditions. One does not have to have basis functions $\mathbf{u}_i(\mathbf{r})$ which obey the boundary conditions, although it reduces the size of the final matrix if they obey as many as possible in a simple way.

The cylinder has a radius a and the z direction is along the axis of the cylinder $-b<z<b$. We use cylindrical coordinates $\mathbf{r}=(\rho,\theta,z)$. We assume the material is isotropic, so the two transverse sound modes have the same velocity c_t. This model can be applied to polycrystalline solids when the grains are small and randomly oriented. The vector wave equation for frequency ω is

$$0=\rho_m\omega^2\mathbf{u}+\mu\nabla^2\mathbf{u}+(\lambda+\mu)\boldsymbol{\nabla}(\nabla\cdot\mathbf{u}). \tag{11}$$

The boundary conditions are that $0=e_{\rho z}=e_{\rho\theta}=\sigma_{\rho\rho}$ on the surface $\rho=a$, while at $z=\pm b$ the boundary conditions are $0=e_{\rho z}=e_{\theta z}=\sigma_{zz}$. These elastic functions are found in the references. The boundary conditions will be satisfied by a perfect variational solution.

The potential energy for the cylinder has the form

$$V_s=\frac{\rho_m}{2}\int d^3r\{c_\ell^2(\nabla\cdot\mathbf{u})^2+c_t^2[e_{\rho z}^2+e_{\rho\theta}^2+e_{\theta z}^2-4e_{zz}(e_{\rho\rho}+e_{\theta\theta})-4e_{\rho\rho}e_{\theta\theta}]\}, \tag{12}$$

where $c_{\ell,t}$ are the longitudinal and transverse speeds of sound. The calculation proceeds by evaluating the potential energy in Eq. (12) and then solving the eigenvalue equation in Eq. (10).

Reference 9 describes a method of solution which can be applied to any object of any shape. They used the basis set $x^\ell y^m z^n$. This set is not convenient for the cylinder, but the computer does all of the work. Figure 1 shows 12 modes with the lowest frequency for a cylinder of length 44 mm and diameter of 34 mm. Material parameters are the same as in Ref. 4: Young's modulus $E=100$ GPa, $\sigma=0.36$, and mass density $\rho_m=5420$ kg/m^3. The frequency beneath each figure are in kHz. The modes with the lowest frequency are mostly transverse. The first mode is a pure torsional motion.

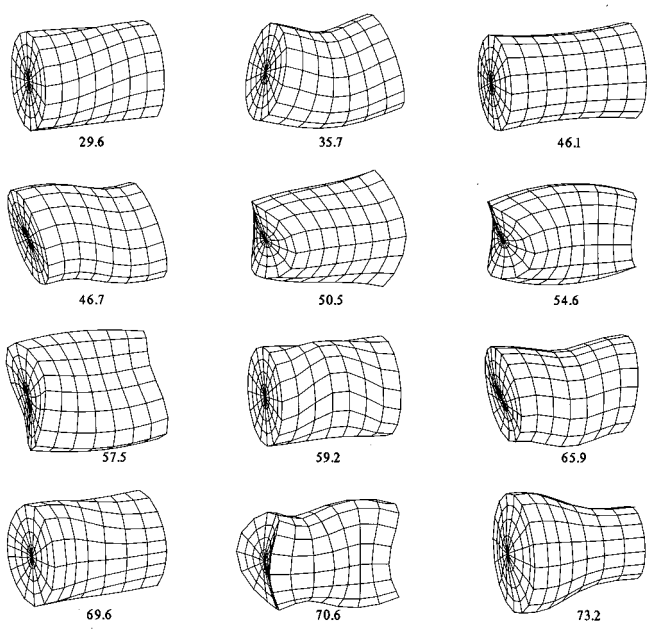

FIG. 1. The 12 modes with the lowest frequency for a cylinder of length 44 mm and diameter of 34 mm. Material parameters are Young's modulus $E=100$ GPa, $\sigma=0.36$, and mass density $\rho_m=5420$ kg/m^3. The frequency beneath each figure is in kHz. The modes with the lowest frequency are mostly transverse. Degenerate modes are omitted.

Among these 12, the only breathing mode has the frequency of 46.1 kHz. It is a simple elongation of the cylinder. Using the $x^\ell y^m z^n$ basis is rather inefficient for our problem since only a small fraction of the modes which are generated are breathing modes. Another difficulty is that in a variational calculation an eigenfunction, which varies by a small factor $O(\varepsilon)$ from the exact eigenfunction, produces an eigenvalue with an error of $O(\varepsilon^2)$. Prior calculations wanted eigenvalues so the set of functions need not be large. Our calculation needs accurate eigenvalues and eigenfunctions, so a larger basis set is required. Therefore we developed a new set of basis functions which are suitable for this problem.

III. BASIS FUNCTIONS

The usual way to solve the vector wave equation is to start with the scalar Helmholtz equation

$$0=[\omega^2+v^2\nabla^2]\phi(\mathbf{r}), \tag{13}$$

where v is a velocity. For the cylinder these are the functions

$$\phi(\mathbf{r})=e^{il\theta}J_\ell(q\rho)\cos(kz), \tag{14}$$

$$\omega^2=v^2(k^2+q^2). \tag{15}$$

Our interest is in the breathing modes of the cylinder, so we take $\ell=0$.

The process for finding the solutions to the vector wave equation are given in Morse and Feshbach.[6] We use the fact that $J_0(z)' = -J_1(z)$:

(1) Longitudinal solutions are given by $\mathbf{u}_\ell = \nabla\phi$, which for $\ell = 0$ have the form

$$\mathbf{u}_\ell(\mathbf{r}) = -\hat{r}_q J_1(qr)\cos(kz) + \hat{z}kJ_0(qr)\sin(kz). \tag{16}$$

This mode has the dilation $\nabla\cdot\mathbf{u}_\ell = -(q^2+k^2)J_0(qr)\cos(kz)$.

(2) The first transverse wave is $\mathbf{u}_{t1} = \nabla\times(\hat{z}\phi)$. Starting with $\phi = J_0(qr)\sin(kz)$ gives

$$\mathbf{u}_{t1}(\mathbf{r}) = -\hat{\theta}\frac{d\phi}{dr} = \hat{\theta}qJ_1(qr)\sin(kz). \tag{17}$$

This mode satisfies $\nabla\cdot\mathbf{u}_{t1} = 0$.

(3) The second transverse wave is given by $\mathbf{u}_{t2} = \nabla\times[\nabla\times(\hat{z}\phi)]$. Starting with $\phi = J_0(qr)\sin(kz)$ gives

$$\mathbf{u}_{t2} = \hat{r}\frac{d^2\phi}{dr\,dz} - \frac{\hat{z}}{r}\frac{d}{dr}\left(r\frac{d\phi}{dr}\right) \tag{18}$$

$$= \hat{r}kqJ_1(qr)\cos(kz) + \hat{z}q^2J_0(qr)\sin(kz). \tag{19}$$

This mode satisfies $\nabla\cdot\mathbf{u}_{t2} = 0$.

The second solution Eq. (17) is a pure torsional mode. It can be made to satisfy all of the stress-free boundary conditions at $z = \pm b$ by choosing $k \equiv k_n = \pi(2n+1)/(2b)$. The choice of q is given by the zeros $\lambda_{\ell\alpha}$ of the Bessel function $0 = J_\ell(\lambda_{\ell\alpha})$. For each ℓ there are an infinite number of α's which satisfy these equations. For the torsional modes we choose $J_2(q_\alpha a) = 0$, which means that $q_\alpha = \lambda_{2\alpha}/a$. This solution is in standard books. There is also a torsional solution give by the unrenormalized eigenfunction

$$\mathbf{u}_{t1}(\mathbf{r}) = \hat{\theta}r\sin(k_n z), \tag{20}$$

which has an eigenfrequency $\omega_n = \pi c_t(2n+1)/(2b)$. For $n=0$ this formula predicts $f_0 = \omega_0/(2\pi) = 29.6$ kHz, which is the first mode shown in Fig. 1.

The second transverse mode $\mathbf{u}_{t2}$ and the longitudinal mode $\mathbf{u}_\ell(\mathbf{r})$ both have vector components in the two directions $(\hat{\rho},\hat{z})$. They mix in the cylinder, and the breathing modes are a mix of these two kinds of modes.

The solutions for the cube provide valuable lessons. Using basis functions such as $\sin(k_n z), \cos(k_n z), k_n = \pi(2n+1)/(2b)$ gives a potential term V_s which is exactly separable when doing the Rayleigh–Ritz method. However, the resulting solutions do not obey the boundary conditions. Demarest[12] showed that using Legendre polynomials $P_n(x/b)$ as the basis gives a matrix for V_s that is not separable, but whose eigenfunctions do satisfy the boundary conditions. The message in the present problem, for the cylinder, is that one cannot use Bessel functions as the basis since they give solutions that are also exactly separable and do not satisfy the boundary conditions. Instead, we must find the cylindrical equivalent of Legendre functions. This feature seems to be required to obtain the desired boundary conditions. For the cylinder, the Legendre functions work in the z direction. However, in the radial direction other functions are required, which are normalized according to

$$\int_0^a \rho\,d\rho\,R_m(\rho)R_n(\rho) = a^2\delta_{nm}N_m. \tag{21}$$

Bessel functions obey these relations, but they do not give us the variational mixture needed to get the right answer. Instead, we created a new set of polynomials for this problem. They are modeled after the Legendre polynomials in that one set $R_{2n}(x), x = \rho/a$, contain only even polynomials, while a companion set $S_{2n+1}(x)$ contain only odd polynomials. They are normalized to $R_{2n}(1) = 1, S_{2n+1}(1) = 1$, and obey the orthogonality relations

$$\int_0^1 x\,dx\,R_{2n}(x)R_{2m}(x) = \delta_{nm}\frac{1}{4n+2}, \tag{22}$$

$$\int_0^1 x\,dx\,S_{2n+1}(x)S_{2m+1}(x) = \delta_{nm}\frac{1}{4n+4}, \tag{23}$$

$$R_0 = 1,\ R_2 = 2x^2-1,\ R_4 = 6x^2(x^2-1)+1, \tag{24}$$

$$S_1 = x,\ S_3 = x(3x^2-2),\ S_5 = x(10x^4-12x^2+3), \tag{25}$$

$$R_{2n} = 2xS_{2n-1} - R_{2n-2},$$

$$S_{2n+1} = \frac{1}{n+1}[(2n+1)R_{2n} - nS_{2n-1}]. \tag{26}$$

The two sets of functions R_{2n}, S_{2n+1} are not mutually orthogonal, but we do not mix them. Since we take their derivatives we need the following relations:

$$\frac{dR_0}{dx} = 0,\ \frac{dR_2}{dx} = 4S_1,\ \frac{dR_4}{dx} = 8S_3 + 4S_1, \tag{27}$$

$$\frac{d}{dx}R^{2n} = 4x(2n-1)R_{2n-2} + \frac{d}{dx}R_{2n-4}, \tag{28}$$

$$\frac{dS_1}{dx} = R_0,\ \frac{dS_3}{dx} = \frac{1}{2}[9R_2 + 5R_0],$$

$$\frac{dS_5}{dx} = \frac{1}{3}[25R_4 + 21R_2 + 5R_0], \tag{29}$$

$$\frac{S_1}{x} = R_0,\ \frac{S_3}{x} = \frac{1}{2}[3R_2 - R_0],$$

$$\frac{S_5}{x} = \frac{1}{3}[5R_4 - 3R_2 + R_0]. \tag{30}$$

One cannot use a state $P_0(z)$ for u_z since that would have the cylinder undergoing center-of-mass motion. Another feature emphasized by Demarest[12] is the symmetry of the modes. If one has odd polynomials in one direction they are coupled with even polynomials in the other direction. These rules guide us in the choice of basis functions. Our final choice is made to fit the boundary conditions, which are explained in Sec. IV. The ansatz wave function is constructed assuming that the maximum polynomial is Nth order, where N is an odd integer. If the variables are (ρ, z') then $x = \rho/a, z = z'/b$. It is also useful to use normalized polynomials which are defined as

$$p_{\ell}(z)=\sqrt{\frac{2\ell+1}{2}}P_{\ell}(z), \tag{31}$$

$$r_n(x)=\sqrt{2(n+1)}\begin{Bmatrix}R_n(x)\\ S_n(x)\end{Bmatrix}. \tag{32}$$

The symbol r_n denotes the normalized R_n or S_n depending upon whether n is even or odd. The eigenfunction expansion for $N=5$ is

$$\mathbf{u}(\mathbf{r})=\hat{\rho}u_\rho+\hat{z}u_z=\sum_{\ell} A_{\ell}\mathbf{u}_{\ell}(\mathbf{r}), \tag{33}$$

$$u_\rho=p_0(z)[A_{10}r_1(x)+A_{30}r_3(x)+A_{50}r_5(x)]+p_2(z)\times[A_{12}r_1(x)+A_{32}r_3(x)]+A_{14}p_4(z)r_1(x), \tag{34}$$

$$u_z=p_1(z)[A_{01}r_0(x)+A_{21}r_2(x)+A_{41}r_4(x)]+p_3(z)\times[A_{03}r_0(x)+A_{23}r_2(x)]+A_{05}p_5(z)r_0(x), \tag{35}$$

where $\mathbf{u}_{\ell}(\mathbf{r})$ are the normalized functions such as $p_0(z)r_3(x)$. Polynomials are retained up to a combined fifth order in the above example. For actual numerical work we retained polynomials up to 13th order, but the above formulas are presented as an example. Also, it was imperative to have analytical results for the interactions in order to check and test the computer code on small values of N.

Using these functions, we can construct the various stress tensor components

$$e_{\rho z}=r_1(x)p_1(z)\left[\frac{\sqrt{3}}{b}(\sqrt{5}A_{12}+\sqrt{9}A_{14})+\frac{2}{a}(\sqrt{6}A_{21}+\sqrt{10}A_{41})\right]+r_3(x)p_1(z)\left[\frac{\sqrt{15}}{b}A_{32}+\frac{\sqrt{80}}{a}A_{41}\right]+r_1(x)p_3(z)\left[\frac{\sqrt{63}}{b}A_{14}+\frac{\sqrt{24}}{a}A_{23}\right], \tag{36}$$

$$e_{zz}=\frac{1}{b}[r_0p_0(\sqrt{3}A_{01}+\sqrt{7}A_{03}+\sqrt{11}A_{05})+\sqrt{5}r_0p_2(z)\times(\sqrt{7}A_{03}+\sqrt{11}A_{05})+r_2(x)p_0(z)(\sqrt{3}A_{21}+\sqrt{7}A_{23})+\sqrt{35}A_{23}r_2(x)p_2(z)+\sqrt{99}A_{05}r_0p_4(z)+\sqrt{3}A_{41}r_4(x)p_0], \tag{37}$$

$$e_{\rho\rho}=\frac{1}{a}\left[r_0p_0\left(\sqrt{2}A_{10}+5A_{30}+5\sqrt{\frac{2}{3}}A_{50}\right)+r_0p_2(z)\times(\sqrt{2}A_{12}+5A_{32})+\sqrt{2}A_{14}r_0p_4(z)+r_2(x)p_0(3\sqrt{3}A_{30}+7\sqrt{2}A_{50})+3\sqrt{3}A_{32}r_2(x)p_2(z)+5\sqrt{\tfrac{10}{3}}A_{50}r_4(x)p_0\right], \tag{38}$$

$$e_{\theta\theta}=\frac{1}{a}\left[r_0p_0\left(\sqrt{2}A_{10}-A_{30}+\sqrt{\frac{2}{3}}A_{50}\right)+r_0p_2(z)(\sqrt{2}A_{12}-A_{32})+\sqrt{2}A_{14}r_0p_4(z)+r_2(x)p_0(\sqrt{3}A_{30}-\sqrt{2}A_{50})+\sqrt{3}A_{32}r_2(x)p_2(z)+\sqrt{\frac{10}{3}}A_{50}r_4(x)p_0\right]. \tag{39}$$

Using these results, the kinetic and potential energy terms are

$$\frac{2K_s}{\rho_m}=A_{10}^2+A_{30}^2+A_{50}^2+A_{12}^2+A_{32}^2+A_{14}^2+A_{01}^2+A_{03}^2+A_{05}^2+A_{21}^2+A_{41}^2+A_{23}^2, \tag{40}$$

$$\frac{2V_s}{\mu}=s\left\{\left[\frac{2}{a}(\sqrt{2}A_{10}+\sqrt{4}A_{30}+\sqrt{6}A_{50})+\frac{1}{b}(\sqrt{3}A_{01}+\sqrt{7}A_{03}+\sqrt{11}A_{05})\right]^2+\left[\frac{2}{a}(\sqrt{2}A_{12}+\sqrt{4}A_{32})+\frac{\sqrt{5}}{b}(\sqrt{7}A_{03}+\sqrt{11}A_{05})\right]^2+\left[\frac{\sqrt{120}}{a}A_{50}+\frac{\sqrt{3}}{b}A_{41}\right]^2+\left[\frac{2}{a}(\sqrt{12}A_{30}+\sqrt{18}A_{50})+\frac{1}{b}(\sqrt{3}A_{21}+\sqrt{7}A_{23})\right]^2+\left[\frac{\sqrt{8}}{a}A_{14}+\frac{\sqrt{99}}{b}A_{05}\right]^2+\left[\frac{\sqrt{48}}{a}A_{32}+\frac{\sqrt{35}}{b}A_{23}\right]^2\right\}+\left[\frac{\sqrt{3}}{b}(\sqrt{5}A_{12}+3A_{14})+\frac{2}{a}(\sqrt{6}A_{21}+\sqrt{10}A_{41})\right]^2+\left[\frac{\sqrt{15}}{b}A_{32}+\frac{\sqrt{80}}{a}A_{41}\right]^2+\left[\frac{\sqrt{63}}{b}A_{14}+\frac{\sqrt{24}}{a}A_{23}\right]^2-\frac{8}{ab}[\sqrt{2}(\sqrt{3}A_{01}+\sqrt{7}A_{03}+\sqrt{11}A_{05})(A_{10}+\sqrt{2}A_{30}+\sqrt{3}A_{50})+\sqrt{10}(A_{12}+\sqrt{2}A_{32})(\sqrt{7}A_{03}+\sqrt{11}A_{05})+2\sqrt{105}A_{32}A_{23}+(2\sqrt{3}A_{30}+3\sqrt{2}A_{50})(\sqrt{3}A_{21}+\sqrt{7}A_{23})+3\sqrt{22}A_{14}A_{05}+3\sqrt{10}A_{50}A_{41}]-\frac{4}{a^2}[(\sqrt{2}A_{10}+\sqrt{4}A_{30}+\sqrt{6}A_{50})^2+(\sqrt{2}A_{12}+\sqrt{4}A_{32})^2+2A_{14}^2], \tag{41}$$

where $s=(c_\ell/c_t)^2$. Starting from these relations, the Rayleigh–Ritz method, Eq. (10), can be used to reduce them to a matrix eigenvalue equation which is solved on the computer. This procedure produces a set of eigenfrequencies ω_i and eigenvectors $A_n^{(i)}=(A_{10}^i,A_{30}^i,A_{50}^i,\cdots,A_{23}^i)$. The eigenvectors are orthogonal

$$\delta_{ij}=\sum_n A_n^{(i)}A_n^{(j)}. \tag{42}$$

The eigenfrequencies can be used to construct the eigenmodes of the cylinder

$$\mathbf{U}_i(\mathbf{r})=\sum_\ell A_\ell^{(i)}\mathbf{u}_\ell(\mathbf{r}), \tag{43}$$

$$\delta_{ij}=\int_0^1 x\,dx\int_{-1}^1 dz\,\mathbf{U}_i(\mathbf{r})\cdot\mathbf{U}_j(\mathbf{r}). \tag{44}$$

These modes are used in discussing the response to the sudden heating.

IV. BOUNDARY CONDITIONS

The vibrations of the cylinder were found in the previous section. They are now used to calculate the response of the cylinder to a pulse of current. The usual current pulse for testing is a ''4–10,'' which means that it rises to its maximum value in 4 μs and decays to half its value in 10 μs. A pulse shape which does this approximately is

$$F(t)=t\exp(-t/\tau), \tag{45}$$

where the constant $\tau=4$ μs. Joule heating in the pulse raises the temperature according to $C\,dT/dt=W_0F(t)$, where W_0 is the power and C is the heat capacity. So the rise in temperature is the integral of $F(t)$ which gives

$$T(t)=\Delta Tf(t), \tag{46}$$

$$f(t)=1-e^{-t/\tau}(1+t/\tau), \tag{47}$$

where ΔT is the final temperature rise caused by the current pulse. Eventually the system will cool down, but that is on a much larger time scale than the current pulse. The stresses in the two directions are

$$\sigma_{zz}=\lambda\boldsymbol{\nabla}\cdot\mathbf{u}+2\mu\frac{\partial u_z}{\partial z}-3K\alpha\Delta Tf(t), \tag{48}$$

$$\sigma_{\rho\rho}=\lambda\boldsymbol{\nabla}\cdot\mathbf{u}+2\mu\frac{\partial u_\rho}{\partial \rho}-3K\alpha\Delta Tf(t), \tag{49}$$

where α is the coefficient of linear expansion, and λ, μ, and K are elastic moduli defined in the Appendix. For a long period, after the system has stopped oscillating, these stresses must vanish. In that case the only solution to these equations for $t\to\infty$ are

$$\frac{\partial u_z}{\partial z}=\frac{\partial u_\rho}{\partial\rho}=\alpha\Delta T, \tag{50}$$

$$\mathbf{u}(\mathbf{r},\infty)=\mathbf{r}\alpha\Delta T=\alpha\Delta T[a\hat{\rho}S_1(x)P_0(z)+b\hat{z}R_0(x)P_1(z)] \tag{51}$$

$$=\alpha\Delta T\left[\frac{a\hat{\rho}}{\sqrt{2}}r_1(x)p_0(z)+\frac{b\hat{z}}{\sqrt{3}}r_0(x)p_1(z)\right]. \tag{52}$$

The equations of motion in Cartesian coordinates are

$$\rho_m\frac{\partial^2}{\partial t^2}u_i(\mathbf{r},t)=\sum_j\frac{\partial}{\partial x_j}\sigma_{ij}. \tag{53}$$

The source term for the elastic oscillation is the current pulse, which causes the cylinder to start expanding. The Joule heating, which causes the expansion, enters into the diagonal stresses σ_{ii}. The heating is assumed to be uniform so that its spatial derivative is zero. In that case it appears to drop out of the calculation. Vojta and Clarke introduced one way of avoiding this problem, and here we introduce another. Our method is to assume the existence of a source term in the dynamical equation. Since the spatial derivative does not affect the time response, this source term must be proportional to $3K\alpha\Delta Tf(t)$. The constant of proportionality is chosen so that the displacement $\mathbf{u}(\mathbf{r},t)$ goes to Eq. (51) in the limit of infinite time. So we solve the equation

$$\rho_m\frac{\partial^2}{\partial t^2}\mathbf{u}(\mathbf{r},t)=\mu\nabla^2\mathbf{u}+(\lambda+\mu)\boldsymbol{\nabla}(\boldsymbol{\nabla}\cdot\mathbf{u})+\rho_m\Lambda(\mathbf{r})f(t), \tag{54}$$

$$\mathbf{u}(\mathbf{r},t)=\sum_i C_i(t)\mathbf{U}_i(\mathbf{r}), \tag{55}$$

where $\mathbf{U}_i(\mathbf{r})$ are the eigenfunctions of frequency ω_i found above by the Demarest method. The coefficients $C_i(t)$ need to be determined, as does the coefficient $\Lambda(\mathbf{r})$. The above equation is solved using a Laplace transform. Because of the form for $f(t)$ the displacement $\mathbf{u}(\mathbf{r},t=0)=0$, as does its first time derivative. In this case the above equation is

$$\tilde{C}_i(p)=\int_0^\infty dt\,e^{-pt}C_i(t), \tag{56}$$

$$\sum_i(p^2+\omega_i^2)\tilde{C}_i(p)\mathbf{U}_i(\mathbf{r})=\Lambda(\mathbf{r})\tilde{f}(p), \tag{57}$$

$$\tilde{f}(p)=\frac{1}{p[1+p\tau]^2}, \tag{58}$$

where $\tilde{C}_i(p),\tilde{f}(p)$ are the Laplace transform of the various functions. The solution for $\tilde{C}_i$ has the form

$$\tilde{C}_i(p)=c_i\frac{\omega_i^2}{p^2+\omega_i^2}\tilde{f}(p), \tag{59}$$

$$c_i=\frac{1}{\omega_i^2}\int d^3r\,\mathbf{U}_i(\mathbf{r})\cdot\Lambda(\mathbf{r}). \tag{60}$$

The inverse Laplace transform gives

$$C_i(t)=c_i\left[1-\frac{(\omega_i\tau)^2}{1+(\omega_i\tau)^2}e^{-t/\tau}\left(1+\frac{t}{\tau}+\frac{2}{1+(\omega_i\tau)^2}\right)-\frac{\cos(\omega_it-2\theta_i)}{1+(\omega_i\tau)^2}\right], \tag{61}$$

$$\tan(\theta_i)=\omega_i\tau. \tag{62}$$

The constant c_i has been introduced, which needs to be determined. The key is that $C_i(t=\infty)=c_i$ so that

$$\mathbf{u}(\mathbf{r},t=\infty)=\sum_i c_i\mathbf{U}_i(\mathbf{r})=\mathbf{r}\alpha\Delta T, \tag{63}$$

$$c_i=\alpha\Delta T\int d^3r\,\mathbf{U}_i\cdot\mathbf{r}, \tag{64}$$

$$c_i=\alpha\Delta T\left(\frac{a}{\sqrt{2}}A_{10}^{(i)}+\frac{b}{\sqrt{3}}A_{01}^{(i)}\right). \tag{65}$$

The last equation completes the derivation. The vibrations of the cylinder are given by Eq. (55), where the amplitudes are given in Eq. (61) in terms of the coefficients c_i defined in the above equation.

As a check on the result, take the second time derivative of Eq. (61) and find

$$\frac{\partial^2}{\partial t^2}C_i(t)=\omega_i^2[c_if(t)-C_i(t)]. \tag{66}$$

Compare this formula to the differential equation (54) which gives

$$\Lambda(\mathbf{r})=\sum_i c_i\omega_i^2\mathbf{U}_i(\mathbf{r}), \tag{67}$$

which agrees with Eq. (60). The derivation is self-consistent, in that one can find a time-independent function $\Lambda(\mathbf{r})$ which generates the correct static displacements at large time.

Equation (61) has two interesting limits: (1) The *adiabatic limit* is when $\omega_i\tau\gg1$. In this case

$$C_i(t)\approx c_if(t). \tag{68}$$

There is no oscillations since the current pulse was slow in time. (2) The other limit is when $\omega_i\tau\ll1$ in which case

$$C_i(t)\approx c_i[1-\cos(\omega_i t)]. \tag{69}$$

Here the pulse is in the *sudden approximation*, and the response is a pure oscillation. In the present case with $\tau=4\ \mu$s most of the elastic modes are in the adiabatic limit and induce no significant oscillation. A very useful quantity is

$$d_i=\frac{c_i}{1+(\omega_i\tau)^2}, \tag{70}$$

which is the coupling of a mode to the oscillatory term $\cos(\omega_i t-2\theta_i)$. The denominator reduces this coupling for modes of higher frequency.

V. COMPARISON TO PRIOR RESULTS

The above equations were put on the computer and calculated for a ZnO arrester. The parameters are used from Ref. 4: $a=17$ mm, $b=22$ mm, $E=100$ GPa, and $\sigma=0.36$. The calculated speeds of sound are: $c_t=2.60$ km/s and $c_\ell=5.57$ km/s. The frequencies ω_i (in units of 10^6 rad/s), $f_i=\omega_i/(2\pi)$ in units of kHz, and constants c_i, d_i are shown in Table I for the lowest six modes. These modes have the largest values of d_i. Note that all of the modes have $\omega_i\tau>1$. If $\omega_i\tau\ll1$ then the system responds in the sudden approximation. If $\omega_i\tau\gg1$ then the system responds adiabatically. In practice the lowest modes have $\omega_i\tau\sim1$ while the higher modes are in the adiabatic limit. The values of d_i decline rapidly for modes of higher frequency. The sign of these values is not significant since they are multiplied by the eigenfunctions $\mathbf{U}_i(\mathbf{r})$ which can have either sign.

TABLE I. Second column are lowest six breathing mode frequencies ω_i in 10^6 rad/s of the cylinder of ceramic ZnO with height=44 mm and radius=17 mm. Third column are frequencies $f_i=\omega_i/(2\pi)$ in units of kHz. Fourth and fifth columns are constants c_i and d_i. The strongest coupling is to these modes. All other modes have $d_i\leqslant O(0.1)$

i	ω_i	f_i	c_i	d_i
1	0.290	46.10	−7.84	−3.35
2	0.470	74.84	−1.05	−0.23
3	0.590	93.95	6.55	1.00
4	0.697	110.84	−5.94	−0.68
5	0.749	119.27	9.64	0.97
6	0.840	133.75	7.30	0.59

Figure 2 shows the stress $\sigma_{zz}(\mathbf{r},t)$ as a function of time in microseconds. The three curves are for $z=0$ (solid triangles), $z=b/2$ (open triangles), and $z=b$ (solid triangles), and all are at $\rho=0$. We set $\alpha\Delta T=1$ in making the graphs. The oscillations are not dominated by a single frequency. All modes contribute to the oscillations, with varying applitudes. The temporal behavior is somewhat complicated.

The stress in the first oscillation is the largest in the center of the cylinder ($z=0$) and gradually decreases toward the ends. We have calculated several points between those shown in order to ascertain that the trend is monotonic. These curves are not shown to avoid cluttering the figure. This negative oscillation is a compressive stress. It occurs when the cylinder heats up rapidly and starts to thermally

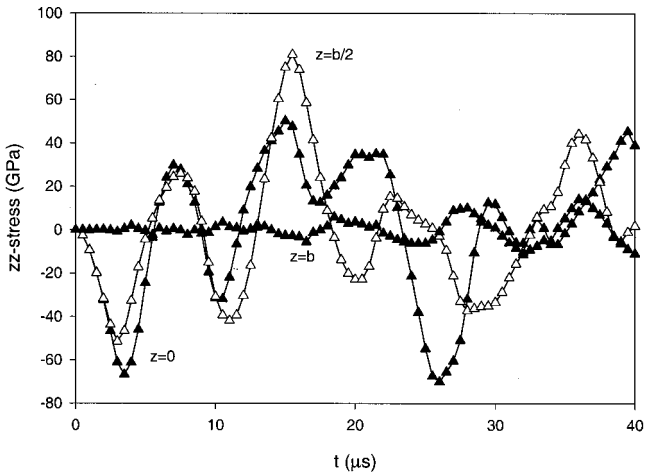

FIG. 2. The value of the stress $\sigma_{zz}(t)$ from a 4–10 pulse calculated assuming $\alpha\Delta T=1$ along the axis $\rho=0$ at the points $z=0, b/2, b$. Here $H=44$ mm, $D=34$ mm. The curve with solid triangles is at $z=0$, in the center of the cylinder. The curve with open triangles is $z=b/2$ at the 1/4 and 3/4 point. The first oscillation is compressive, and the stress is largest at the center $z=0$. The next oscillation at $t=8\ \mu$s has about the same stress at $z=0,b/2$. It is about 10% higher at $z=b/4$: this curve is not shown. It will break under tension at anyplace along $-b/2\leqslant z\leqslant b/2$. The next big oscillation is at $t=17\ \mu$s, and the stress is largest at $z=b/2$. The other curve is at the end of the cylinder.

expand. The expansion has not yet occurred so the cylinder is under compression. It can break, and in this case would break in the center.

The second large oscillation at about 17 μs has a positive amplitude. It is the first expansion of the cylinder, which overshoots the equilibrium point. In this case the largest *zz* stress is at the point $z=b/2$, which is at the 1/4 or 3/4 point along the length of the cylinder. The breaking point under tension is less than the breaking stress under compression. The cylinder could break at this point if it did not break in the first oscillation. In this case the breaking would occur at the 1/4 or 3/4 point. These results are in very good agreement with those in Ref. 4. They showed only the curve we label $z=b/2$, which they asserted had the largest value of *zz* stress. Their curve is very similar to our curve, so we confirm their results. However, the cylinder will not always break at the 1/4 or 3/4 point since it could break in the first oscillation under compression. Experimentally it is found that varistors usually break in the center, and the break is along a plane perpendicular to the *z* axis.

The line in Fig. 2 with solid triangles and small amplitude is the stress $\sigma_{zz}(t)$ evaluated at the end of the cylinder: $(\rho=0,\ z=b)$. This stress is zero if the boundary conditions are obeyed perfectly. In the variational calculation the end stress is quite small but not zero. Increasing the degree N of the polynomial causes this stress to become increasing small.

In doping these calculations we set $\alpha\Delta T=1$. In practice this dimensionless quantity is $O(10^{-4})$. The dynamic stresses are of order mega-Pascal rather than giga-Pascal.

VI. ELASTIC MEASUREMENTS

A station arrester of ZnO was obtained. It is a commercial unit manufactured by the Ohio Brass Company. Varistors are ZnO ceramics with additives of other metal oxides, each at the level of 1%. Each manufacturer has a different set of additives, which is proprietary.

The frequencies of the lowest normal modes were measured. An HP 3325B frequency synthesizer with frequency resolution of 1 μHz is used to excite the sample via a gold plated PVDF transducer. The sample response is monitored with a similar transducer. The signal is amplified and sent to a Stanford Research SR844 RF lock-in amplifier and recorded on a Sun workstation. The Lorentzian peaks are then fitted, which extracts the center frequency. More details are given in Ref. 15.

The ZnO cylinder had $D=4.295$ cm, $H=4.201$ cm, and density $\rho_m=5.350\ \mathrm{gm/cm^3}$. The frequencies were fit well by the parameters of $E=1.135$ Mbar and Poisson ratio $\sigma=0.391$. These cylinders have aluminum electrodes on the end, and are then coated. The electrodes and coatings were etched away, leaving a cylinder of pure ZnO ceramic. This cylinder has $D=4.089$ cm, $H=4.153$ cm, and density $\rho_m=5.575\ \mathrm{gm/cm^3}$. The lowest frequency modes were measured, and the *xyz* code was used to fit them, adjusting only two parameters, which gave $E=1.1349$ Mbar and $\sigma=0.3378$. The major change from the coated cylinder was the Poisson ratio. The lowest 15 modes and their calculated values are shown in Table II. Many are degenerate since they have the same value for $\pm n$. The only breathing mode in this list is No. 8. The first cylinder, shown in Fig. 2 and in Table I, had $H>D$ and the first breathing mode was No. 4. Here with $H\sim D$ the first breathing mode has dropped to No. 8.

TABLE II. Observed and calculated frequencies of a ceramic cylinder of ZnO. Fourth column is error, while last column is mode degeneracy.

Mode	Obs-F (kHz)	Calc-F (kHz)	% Difference	Degeneracy
1	33.195	33.207	−0.035	1
2–3	42.375	42.374	0.002	2
4–5	42.597	42.624	−0.064	2
6–7	45.881	45.931	−0.109	2
8	49.420	49.422	−0.004	1
9–10	50.212	50.175	0.073	2
11–12	53.301	53.286	0.028	2
13–14	60.854	60.815	0.065	2
15	63.199	63.242	−0.068	1

The breathing modes were calculated using the basis set with $[p_\ell(z),r_n(x)]$. The same values were used for the size, density, and elastic parameters. These frequencies are shown in Table III, along with the coupling coefficients c_i,d_i. Again only a few modes of small frequency have a significant value of coupling d_i to the induced oscillations. Figure 3 shows the value of the stress σ_{zz} from a 4–10 pulse calculated assuming $\alpha\Delta T=1$ along the axis $\rho=0$ at the points $z=0,b/2,b$. The line with solid triangles is at $z=0$, in the center of the cylinder. The curve with open triangles is $z=b/2$ at the 1/4 and 3/4 point. The first oscillation is compressive, and the stress is largest at the center $z=0$. The next oscillation at $t=8$ μs has about the same stress at $z=0$, $b/2$. It is about 10% higher at $z=b/4$: this curve is not shown. It will break under tension at any place along $-b/2\leqslant z\leqslant b/2$. The next big oscillation is at $t=17$ μs, and the stress is largest at $z=b/2$. Again the other curve with solid triangles is at the ends of the cylinder and this is small, which means the boundary conditions are obeyed approximately.

Figure 4 shows the same results for $\sigma_{\theta\theta}(t)$. The three curves are the points: solid triangles $(\rho=0=z)$, open triangles $(\rho=0,\ z=b/2)$, and solid triangles $(\rho=a/2,\ z=0)$. The curve with $(\rho=0=z)$ has the largest amplitude for all oscillations. In both Figs. 3 and 4, the first large expansion peak occurs at 8–10 μs. For this peak note that $\sigma_{\theta\theta}(t)$

TABLE III. Second column are lowest eight breathing mode frequencies ω_i in 10^6 rad/s of the cylinder of ceramic ZnO with height=41.5 mm and radius=20.45 mm. Third column are frequencies $f_i=\omega_i/(2\pi)$ in units of kHz. Fourth and fifth columns are constants c_i and d_i. The strongest coupling is to the modes 1, 3, and 4.

i	ω_i	f_i	c_i	d_i
1	0.3106	49.43	4.07	1.60
2	0.4239	67.47	−1.15	−0.30
3	0.5649	89.90	−13.47	−2.21
4	0.6855	109.09	−9.87	1.16
5	0.7267	115.65	6.01	0.64
6	0.7792	124.02	−1.34	−0.12
7	0.9421	149.95	−1.02	0.07
8	0.9727	154.81	−1.14	−0.07

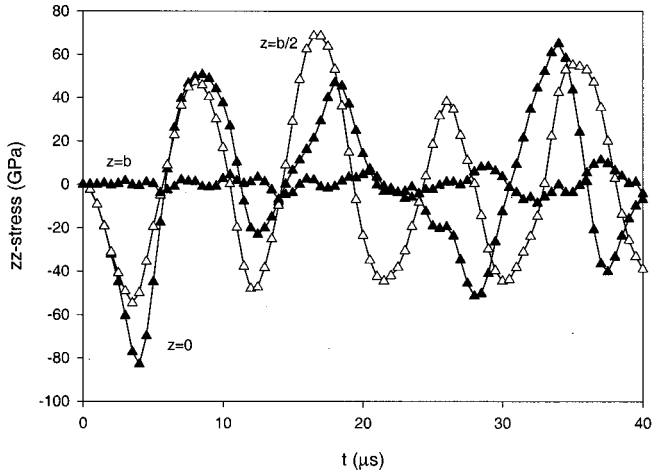

FIG. 3. The value of the stress $\sigma_{zz}(t)$ from a 4–10 pulse calculated assuming $\alpha\Delta T=1$ along the axis $\rho=0$ at the points $z=0,b/2,b$. Here $H=41.53$ mm, $D=40.89$ mm. The curve with solid triangles is at $z=0$, in the center of the cylinder. The curve with open triangles is $z=b/2$ at the 1/4 and 3/4 point. The first oscillation is compressive, and the stress is largest at the center $z=0$. The next oscillation at $t=10$ μs has about the same stress at $z=0,b/2$. It is about 5% higher at $z=b/4$: this curve is not shown. It will break under tension at anyplace along $-b/2\leqslant z\leqslant b/2$. The next big oscillation is at $t=17$ μs, and the stress is largest at $z=b/2$. The other curve is at the end of the cylinder.

$>\sigma_{zz}(t)$. We also calculated $\sigma_{\rho\rho}(t)$. It is identical to $\sigma_{\theta\theta}(t)$ along the line $\rho=0$. Away from that line it is smaller than $\sigma_{\theta\theta}(t)$. So for this case with $H\sim D$ the fracture will be pie shaped rather than along the plane perpendicular to the z axis.

It should be kept in mind that these figures do not apply to an actual arrester, since the calculations were done for a cylinder lacking electrodes.

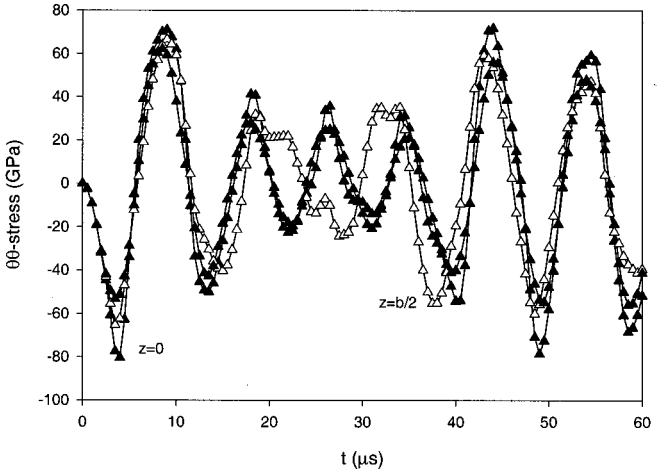

FIG. 4. Time dependent stress $\sigma_{\theta\theta}(t)$ from a 4–10 pulse for the cylinder with $H=41.53$ mm, $D=40.89$ mm. The curve with solid triangles is at point ($\rho=0$, $z=0$); the curve with open triangles is at point ($\rho=0$, $z=b/2$); the other line is at ($\rho=a/2$, $z=0$). The stress is smaller when $\rho\neq 0$ than along the axis with $\rho=0$. The largest stress is found at the point ($\rho=0$, $z=0$).

ACKNOWLEDGMENTS

G.D.M. thanks Dr. Felix Greuter and Dr. Veerle Keppens for discussions on this calculation.

APPENDIX: STRESS AND STRAIN

Here we review some standard relations between the various constants used in stress and strain equations: E is Young's modulus, σ is the Poisson ratio, K is the bulk modulus of elasticity, λ is Lame's constant, μ is the modulus of rigidity, and α is the *coefficient of linear expansion*

$$\mu=\frac{E}{2(1+\sigma)}=\rho c_t^2, \tag{A1}$$

$$K=\frac{E}{3(1-2\sigma)}=\rho\left[c_\ell^2-\frac{4}{3}c_t^2\right], \tag{A2}$$

$$\lambda=K-\frac{2}{3}\mu=\rho(c_\ell^2-2c_t^2)=\frac{\sigma E}{(1+\sigma)(1-2\sigma)}, \tag{A3}$$

$$\sigma=\frac{3K-2\mu}{2(3K+2\mu)}=\frac{\lambda}{2(\lambda+\mu)}, \tag{A4}$$

$$E=\frac{9K\mu}{3K+\mu}=\frac{\mu(3\lambda+2\mu)}{\lambda+\mu}, \tag{A5}$$

$$\rho c_\ell^2=\frac{E(1-\sigma)}{(1+\sigma)(1-2\sigma)}=K+\frac{4}{3}\mu=\lambda+2\mu, \tag{A6}$$

$$\rho\Delta^2=\rho[c_\ell^2-c_t^2]=\frac{E}{2(1+\sigma)(1-2\sigma)}=\lambda+\mu. \tag{A7}$$

The diagonal and off-diagonal stresses are

$$\tau_{ii}=K[\nabla\cdot\mathbf{u}-3\alpha\delta T]+2\mu\left[\frac{\partial u_i}{\partial x_i}-\frac{1}{3}\nabla\cdot\mathbf{u}\right], \tag{A8}$$

$$\tau_{ij}=\mu\left(\frac{du_i}{dx_j}+\frac{du_j}{dx_i}\right). \tag{A9}$$

[1] M. Bartkowiak, M. G. Comber, and G. D. Mahan, J. Appl. Phys. **79**, 8629 (1996).
[2] F. A. Modine, L. A. Boatner, M. Bartkowiak, G. D. Mahan, H. Wang, and R. B. Dinwiddie, Ceram. Trans. **100**, 469 (1999).
[3] A. Vojta and D. R. Clarke, J. Am. Ceram. Soc. **80**, 2086 (1997).
[4] M. Lengauer, D. Rubesa, and R. Danzer, J. Eur. Ceram. Soc. **20**, 1017 (2000).
[5] A. E. H. Love, *A Treatise on the Mathematical Theory of Elasticity* (Dover, New York, 1944), Sec. 201.
[6] P. M. Morse and H. Feshbach, *Methods of Theoretical Physics* (McGraw-Hill, New York, 1953) Vol. II, Sec. 13.3.
[7] H. Reismann and P. S. Pawlik, *Elastokinetics* (West, St. Paul, MN, 1974), Sec. 11.6.
[8] A. C. Eringen and E. S. Suburi, *Elastodynamics* (Academic, New York, 1975) Vol. II, Sec. 8.9.
[9] W. M. Visscher, A. Migliori, T. M. Bell, and R. A. Reinert, J. Acoust. Soc. Am. **90**, 2154 (1991).
[10] H. Ekstein and T. Schiffman, J. Appl. Phys. **27**, 405 (1956).
[11] R. Holland, J. Acoust. Soc. Am. **42**, 988 (1968).
[12] H. H. Demarest Jr., J. Acoust. Soc. Am. **49**, 768 (1971).
[13] I. Ohno, J. Phys. Earth **24**, 355 (1976).
[14] A. Migliori *et al.*, Phys. Rev. B **41**, 2098 (1990).
[15] J. D. Maynard, Phys. Today (January 26, 1996).